metals

MDPI

Article

Relationship between Residual Stress and Net Strain in Low-Temperature Transformation Weldments Considering Microstructure

Jaehee Lee, Youngchai Lee and Changhee Lee *

Division of Materials Science and Engineering, Hanyang University, Seoul 133-791, Korea; ej6320@naver.com (J.L.); yc_lee2015@naver.com (Y.L.)
* Correspondence: chlee@hanyang.ac.kr; Tel.: +82-2-2220-0388

Abstract: Weldments inevitably shrink during cooling from the melt pool. Residual stresses then occur owing to surrounding constraints. Tensile residual stresses in weldments cause various problems, such as deformation and reduction of fatigue strength. Low-temperature transformation (LTT) welding consumables can reduce the tensile residual stress through volume expansion, which accompanies a phase transformation from austenite to martensite. In this study, the relationship between residual stress and net strain was examined, mainly by controlling the martensite start (Ms) temperature, and the result was related to the weld's microstructure. The Ms temperature and the expansion accompanying the phase transformation were analyzed by the dilatometric method. A hole drilling test was carried out to measure the residual stress in the weldments. The highest compressive stress was observed in the most expanded weldment at room temperature, and a linear relationship between the net strain and residual stress was derived. This linear relationship was analyzed with a microstructural approach.

Keywords: low temperature transformation; martensite starting temperature; residual stress; net strain

check for updates

Citation: Lee, J.; Lee, Y.; Lee, C. Relationship between Residual Stress and Net Strain in Low-Temperature Transformation Weldments Considering Microstructure. *Metals* **2021**, *11*, 755. https://doi.org/10.3390/met11050755

Academic Editor: Michal Krzyzanowski

Received: 12 April 2021
Accepted: 30 April 2021
Published: 3 May 2021

Publisher's Note: MDPI stays neutral with regard to jurisdictional claims in published maps and institutional affiliations.

Copyright: © 2021 by the authors. Licensee MDPI, Basel, Switzerland. This article is an open access article distributed under the terms and conditions of the Creative Commons Attribution (CC BY) license (https://creativecommons.org/licenses/by/4.0/).

1. Introduction

Molten steel materials are transformed to δ-ferrite in the initial stage of solidification, then transformed to face-centered cubic (FCC) structured austenite in the middle stage, and finally transformed to the ferritic phase (ferrite, bainite, or martensite) with a body-centered cubic (BCC) structure. Crystallographically, the FCC structure has an atomic packing factor of 74%, denser than the BCC structure's factor of 68%, and so has smaller inter-atomic spacing. Thus, when a FCC structure is transformed to BCC, the volume increases [1–3]. Subsequently, shrinkage occurs while cooling to room temperature. In particular, the welding area undergoes compression and expansion owing to rapid temperature variations and mechanical restraints [4,5]. Residual stresses that inevitably occur during this process cause deformation of the welded part, thereby reducing the integrity of the structure [6]. There are several types of deformation, such as shrinkage deformation, rotational deformation, and bending deformation. However, buckling deformation is the most difficult to correct and requires long working times. Because buckling deformation is caused by the tensile residual stress in the weld, it is essential to study this stress to control the strain.

Recently, low-temperature transformation (LTT) materials, which can reduce residual stress by controlling the martensite start (Ms) temperature, have been actively studied. The LTT material can control the tensile residual stress resulting from contraction of the weld through the expansion accompanying the transformation from austenite (FCC) to martensite (BCC) in the weld metal [7–14]. The LTT welding material contains a martensite structure during the final phase transformation because large amounts of alloying elements are normally added to lower the transformation temperature [15,16].

Numerous studies on controlling the Ms temperature of LTT welding materials have been reported [17–20]. Francis et al. investigated the effect of filler metal transformation

temperature on residual stress in high-strength steel welding [17]. The mechanical properties of high-strength steel plates welded with LTT electrodes were investigated by Özdemir et al. [18]. Martinez et al. showed how metal phase transformations could be used to generate compressive, rather than tensile, residual stress in structural steel weld toes [20]. Gyubaek An et al. investigated effects of high toughness and welding residual stress for unstable fracture prevention [21]. The above studies focused on the characteristics of LTT materials which control the Ms temperature and residual stress, relating mechanical (tensile and fatigue) properties to variations in elemental composition. However, there are insufficient studies on the characteristics of LTT materials considering microstructure and deformation.

In this study, we examined the relationship between residual stress and deformation, considering the microstructure of the LTT weld. Cr and Ni have been adopted as major variables in most LTT production due to efficient reduction of Ms temperature and suitability of mechanical properties within the addition range of 10–14% wt. and 5–11% wt., respectively, and most of them have low carbon content [22–24]. A low carbon content is required to prevent the formation of chromium carbide and to prevent the formation of hard and brittle martensite in the heat affected zone (HAZ). Manganese can act as an efficient austenite stabilizer, but the addition of high manganese can lead to a decrease in toughness. Molybdenum is effective in reduction of Ms temperature, but it is not suitable when it is produced as an actual welding material due to high cost. Therefore, in this study the Ms temperature was changed by adjusting the Cr and Ni content. The relationship between residual stress and deformation was identified through microstructure analysis for each Ms temperature, and the effect of decreasing deformation was verified through actual welding with LTT welding consumables.

2. Materials and Methods

The test samples were fabricated in the form of 1.7 kg ingots using a vacuum induction furnace. Test samples were prepared in an argon atmosphere to prevent oxidation, at a current and voltage of 15 A and 200 V, respectively. To determine the LTT material characteristics, the M_s temperature was calculated from the Cr and Ni content according to the following empirical equation [25]:

$$M_s = 539 - 423C - 30.4Mn - 12.1Cr - 17.7Ni - 7.5Mo \ (wt.\%) \quad (1)$$

Spark emission spectroscopy (QSN750-II, OBLF) was used to analyze the chemical composition of the test samples. The results are shown in Table 1. Cr and Ni equivalents were calculated using a Schaeffler constitution diagram [26]. The gas tungsten arc welding (GTAW) process was performed on a 6 mm ingot plate for the weld simulation, with the corresponding welding conditions listed in Table 2.

A dilatometer test was performed to measure the Ms temperature of each sample. All specimens were austenitized at 1000 °C, based on the results obtained from thermal calculation software. The thermal cycle of the dilatometer test was calculated using the Rosenthal equation [27]:

$$T - T_0 = \frac{qv}{2\pi\lambda t} \exp\left(-\frac{r^2}{4at}\right) \quad (2)$$

where T_0 is initial temperature (°C), T is temperature (°C), q is heat input (J/m), v is travel speed (m/s), λ is thermal conductivity ($Js^{-1}m^{-1}°C^{-1}$), r is radial/lateral distance from weld (m), a is thermal diffusivity (m^2/s), and t is time (s). The sample for the dilatometer test (Theta, Formanex) was machined from the all-weld metal. This sample measured 3 mm in diameter and 10 mm in length. The dilatometer sample was cooled in helium gas atmosphere, and the austenitized temperature was calculated by thermodynamic simulation, performed at 1000 °C. The test conditions were: a heating rate of 50 °C/s, holding temperature of 1000 °C for 30 s, and a cooling rate of 11 °C/s.

Table 1. Chemical compositions and Cr and Ni equivalent (Cr_{eq}/Ni_{eq}) ratios of specimens (wt. %).

Specimen	C (%)	Si (%)	Mn (%)	Mo (%)	Cr (%)	Ni (%)	Cr_{eq}/Ni_{eq} Ratio
LTT A	0.04	0.37	0.98	0.25	10.1	3.7	1.72
LTT B	0.04	0.37	1.00	0.24	11.9	4.8	1.71
LTT C	0.04	0.44	0.99	0.26	13.8	5.7	1.72
LTT D	0.05	0.43	0.93	0.26	14.9	8.3	1.70
LTT E	0.05	0.43	1.00	0.26	19.5	10.1	1.69

Table 2. Welding conditions.

Welding Parameter	Value
Welding type	Bead on plate (autogenous)
Welding current	180 A
Welding voltage	16 V
Travel speed	15 cm/min
Heat input	9 kJ/cm
Plate thickness	6 mm
Shielding gas	Argon
Flow rate of shielding gas	18 L/min

To measure the residual stress of the welding area, a hole drilling test was performed, as shown in Figure 1. There are non-destructive and destructive methods for measuring residual stress. Non-destructive measurement methods include X-ray diffraction and neutron diffraction, and methods for measuring destructive residual stress include hole drilling and nano-indentation [5,28–30]. Among them, the hole drilling method is most suitable in research that requires experimenting with multiple candidate groups because it enables rapid and accurate measurement at an appropriate cost [31]. In addition, it is possible to measure residual stress in a relatively deep place compared to other methods. Holes of 2.1 mm diameter were drilled to a depth of 0.25, 0.50, 0.75, and 1.0 mm, respectively. Residual stresses were obtained by attaching strain gauges to the weldment center, weldment toe, and base metal [32]. For microstructure analysis, the test samples were first polished using #2000 SiC paper and a 1 µm diamond suspension. The microstructure was then observed by etching with 3% Natal and Vilella etchant. The microstructure was analyzed using optical microscopy(OM) and X-ray diffraction (XRD) (X'Pert PRO, PANalytical). Diffraction data were collected by scanning from 40 to 100° with a step size of 0.02° (2θ).

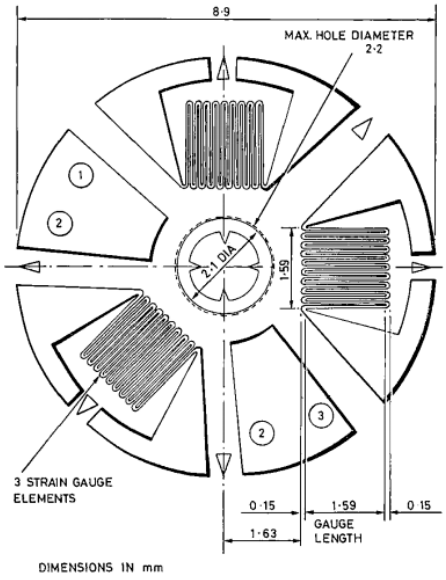


Figure 1. Strain gauge rosette for the hole-drilling method [27].

3. Results and Discussions

Carbon, manganese, nickel, chromium, and molybdenum are the elements commonly used in LTT alloys. However, the addition of carbon and manganese is limited owing to their effect on the weldability of the LTT materials in the weldment. In this study, LTT weldments were designed with varied chromium and nickel content. This material had a composition similar to stainless steel. Therefore, it was possible to secure the ease of microstructure prediction from the alloy design stage by using a Schaeffler diagram, and using the equivalents of Cr and Ni as variables. In particular, the ratio of Cr equivalent to Ni equivalent was controlled, to prevent adverse effects of other elements on the Ms temperature or microstructure. According to Kujanpaa's research on austenitic stainless steel [33], alloys with a Creq/Nieq ratio of approximately 1.55 or more are solidified into primarily ferrite and have greater resistance to high-temperature cracking. For a specimen with a Creq/Nieq ratio of approximately 1.7, no solidification cracking was observed, regardless of the phosphorus and sulfur content [33]. In this study, the Creq/Nieq ratio of the specimens was set to about 1.7, to guarantee the uniformity of the phase fractions and weldability of the material.

Figure 2 shows a graph of net strain versus Ms temperature for LTT welds with a Creq/Nieq ratio, compared with conventional welding consumables.

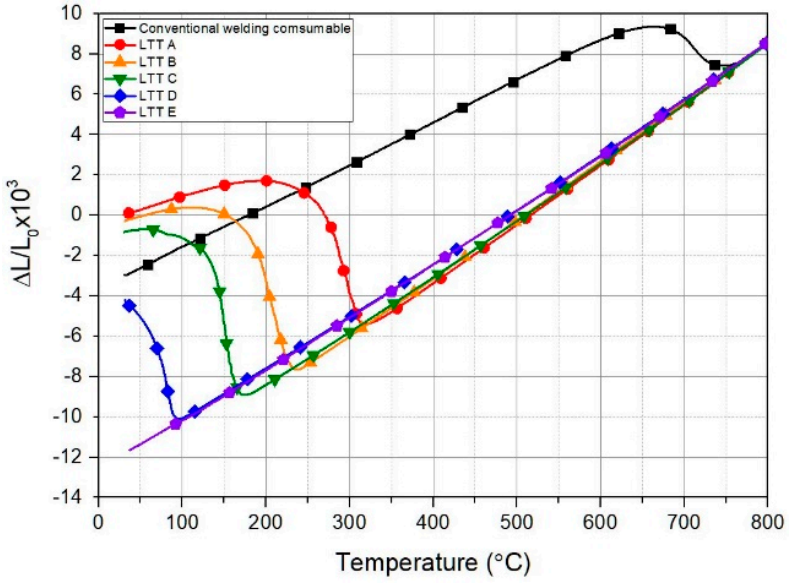


Figure 2. Dilatometric curves of the low-temperature transformation (LTT) A, B, C, D, and E samples.

The Ms temperature is defined as the temperature corresponding to the lowest strain measured during phase transformation, according to the ASTM A1033 standard [34]. In the ASTM measurement method, dilatometer curve noise is not considered in the initial phase transformation state [35]. The cooling curve of the dilatometer graph was analyzed as shown in Figure 3 to calculate the Ms temperature.

Here, ε is the strain value at the Ms temperature converted to room temperature, and H is the maximum expansion point obtained from the Ms and D expansion section [36]; H and D are the volume expansion caused by martensitic transformation and the temperature range that must be cooled to show the maximum volume expansion, respectively. The values of Ms, ε, H, and D obtained from the dilatometer curve analysis of LTT specimens A to E are shown in Table 3.

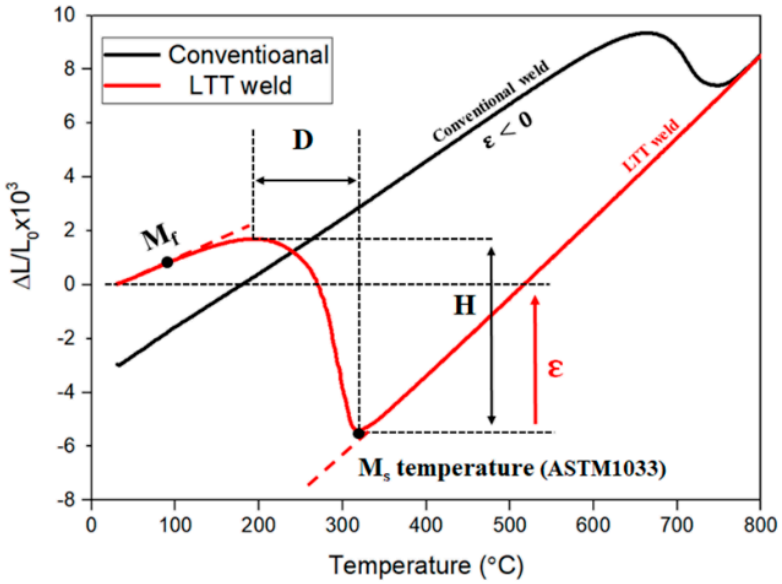


Figure 3. Representation of ε (net strain), H (maximum expansion), and D (expansion section) in dilatometric analysis.

Table 3. Martensite start (Ms) temperatures, and ε, H, and D values of specimens with similar Creq/Nieq ratios.

Specimen	Ms Temperature (°C)	ε ($\Delta L/L_0 \times 10^3$)	H ($\Delta L/L_0 \times 10^3$)	D (°C)
LTT A	319	5.44	7.11	127
LTT B	239	7.37	8.04	127
LTT C	175	8.07	8.20	119
LTT D	92	5.18	>5.18	>92
LTT E	<25	-	-	

All the LTT welds showed relatively low Ms temperatures compared to welds using conventional welding consumables. The Ms temperature of the LTT welds decreased from 319 °C to below room temperature as Creq and Nieq increased, while maintaining the Creq/Nieq ratio at 1.7. The maximum value of net strain was observed for a LTT specimen C with an Ms temperature of 175 °C. On the other hand, the maximum net strain for specimen D and E occurred at temperatures below room temperature, while the maximum expansion point decreased without further expansion. For specimens D and E, the H and D values were not accurately measured because the volume expansion did not reach its maximum value at room temperature. If the expansion section due to the transformation of specimens A, B, and C was applied to specimen D, the point at which the expansion of the volume became maximum due to the martensitic transformation was expected to be about −32 °C. Despite the decrease in Ms temperature, the net strain (ε) showed a tendency to increase and then decrease. From the dilatometer analysis, expansion by phase transformation of the LTT materials used in this study maximized at an Ms temperature of approximately 175 °C. This means that a lower Ms temperature alone did not have a beneficial effect on deformation.

Because the actual deformation of weldments is caused by residual stress, a hole drilling test was carried out to investigate the effect of the Ms temperature on the residual stress. The results of this investigation, with increasing Creq and Nieq, are shown in Figure 4, compared with the residual stress of weldments using conventional welding consumables. The dotted lines in the graph represent the welding toe, and the + and − directions of the y-axis correspond to tensile and compressive residual stress, respectively.

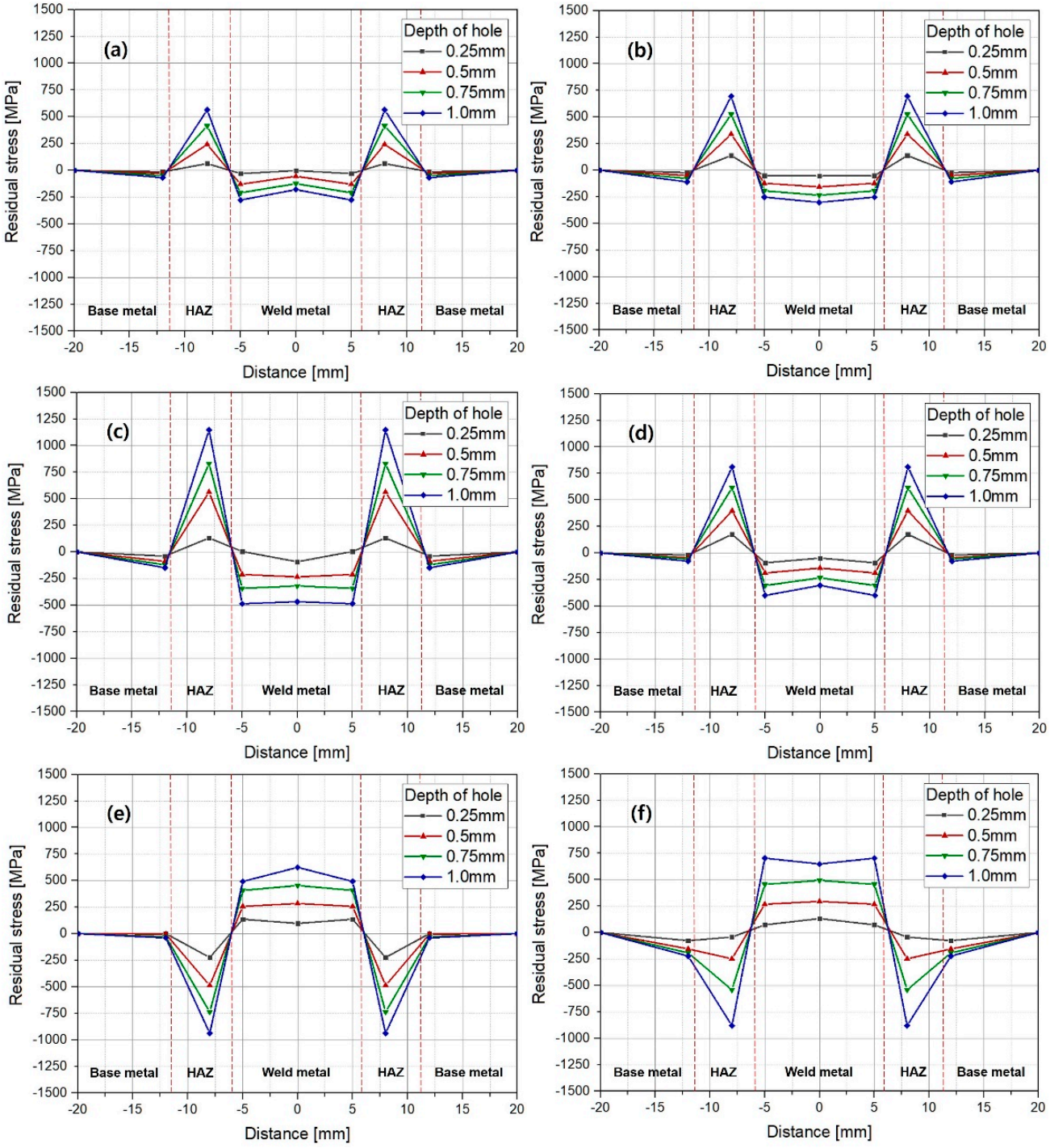


Figure 4. Hole drilling test results: (**a**) LTT A, (**b**) LTT B, (**c**) LTT C, (**d**) LTT D, (**e**) LTT E, and (**f**) conventional welding consumables.

As shown in Figure 4, a tensile residual stress of approximately 550 MPa was obtained in the weld using a conventional welding consumable. In the LTT welds, the residual stress was compressive; however, as the Ms temperature decreased, this compressive residual stress gradually increased and then decreased. This result was similar to the variation in net strain according to the Ms temperature obtained from the dilatometric analysis. The relationship between net strain and residual stress according to the Ms temperature is shown in Figure 5.

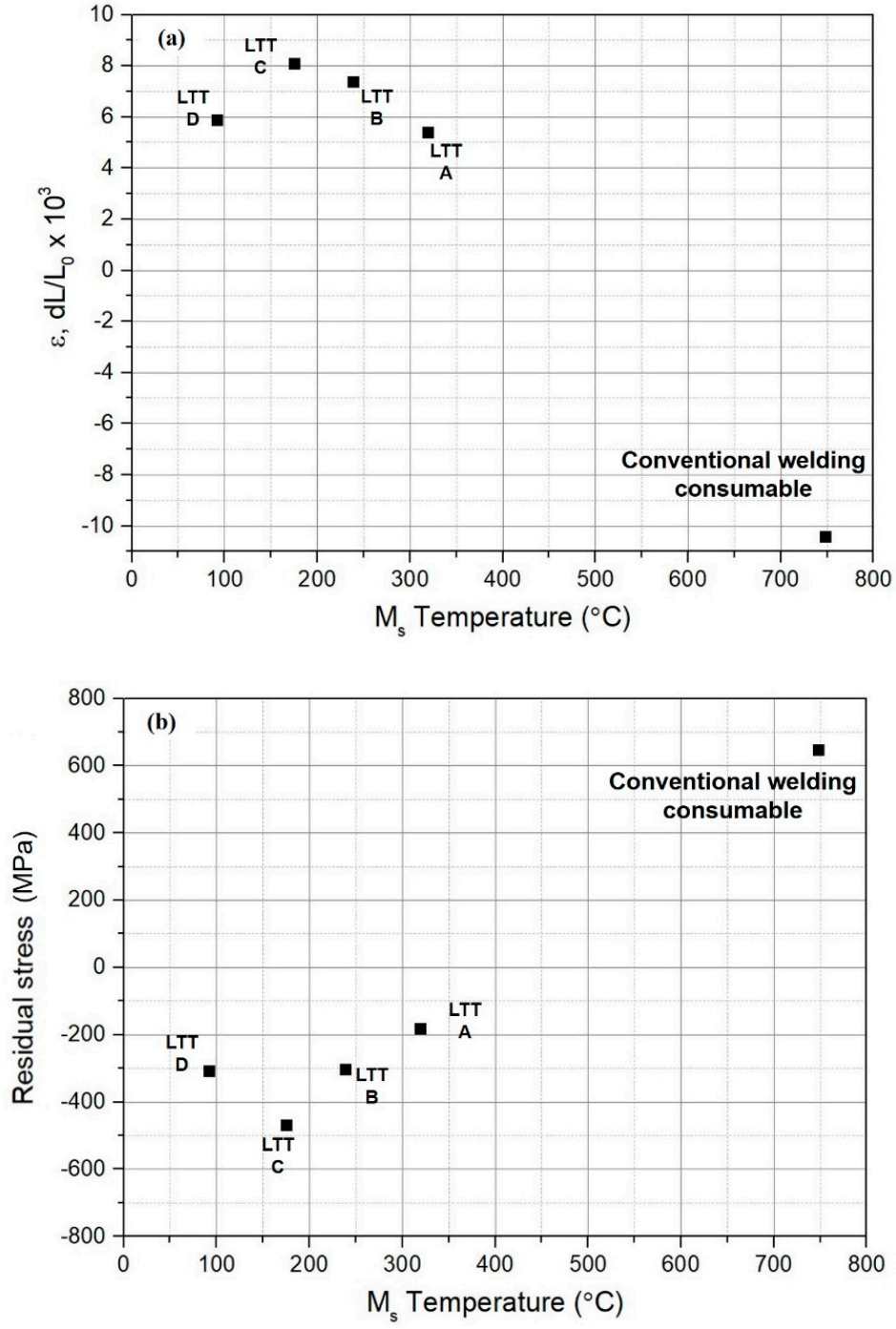


Figure 5. The relationship between Ms temperature and (**a**) net strain, (**b**) and residual stress of LTT weldments.

The residual stress produced an inflection point around 175 °C similar with net strain as the Ms temperature decreased. The point of net strain and residual stress of each specimen were symmetrical as Ms temperature decreased. Figure 5 shows that there was a clear relationship between net strain and residual stress; however, the graph exhibits a different tendency from previous results, which showed that the lower the Ms temperature, the greater was the effect of reducing deformation.

To investigate the metallurgical reason for the presence of the inflection point in the net strain and Ms temperature graph, microstructure analysis was carried out. Microstructure analyses of LTT samples A to E, with different Ms temperatures, were performed, with the results shown in Figure 6.

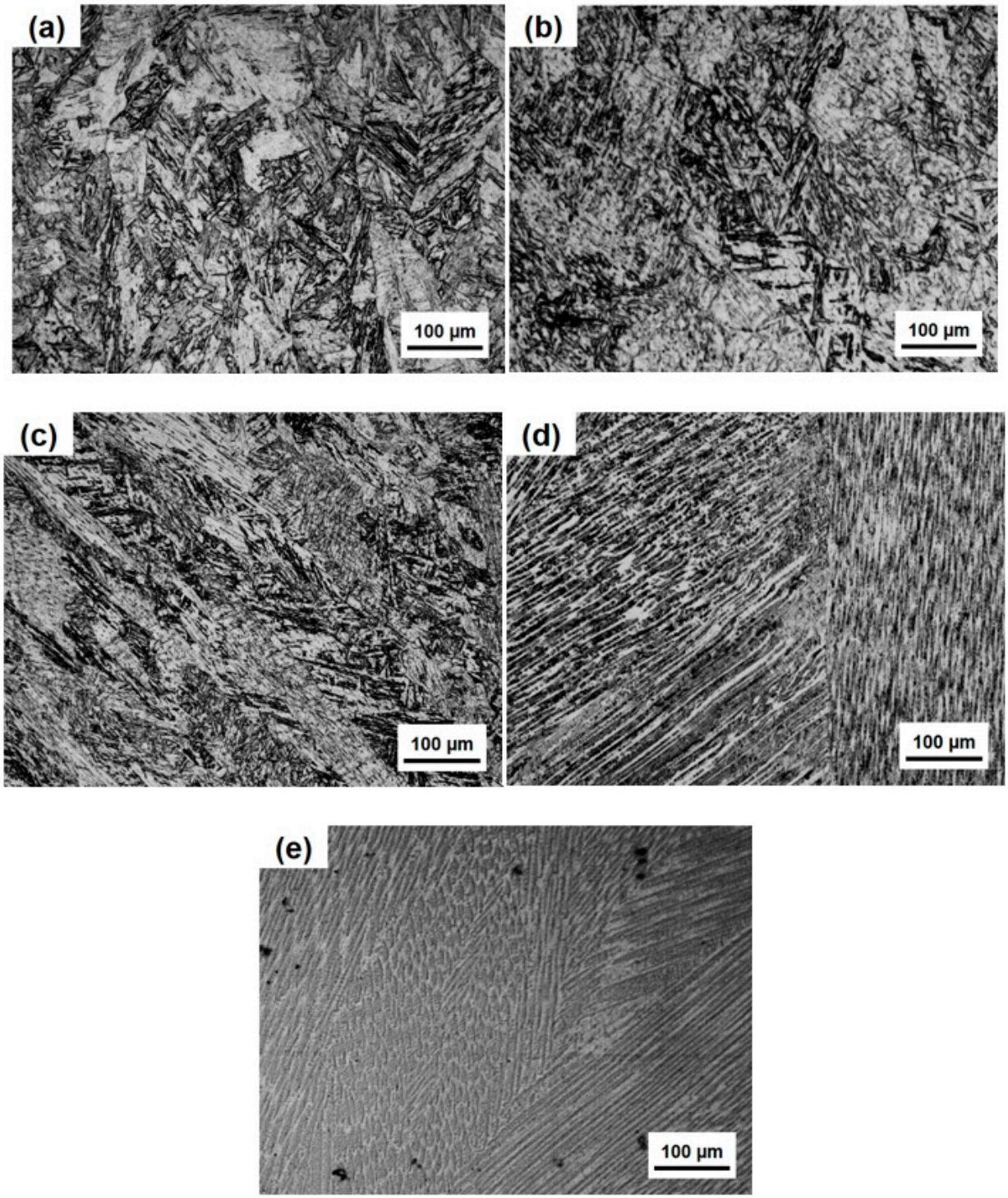


Figure 6. OM images of the samples: (**a**) LTT A, (**b**) LTT B, (**c**) LTT C, (**d**) LTT D, and (**e**) LTT E.

The conventional welding consumable specimen was excluded from the microstructure analysis, because there was no significant correlation with an inflection point. As shown in Figure 6, LTT specimens A to C were transformed to almost 100% martensitic structures. Although the microstructures of the LTT specimens A, B, and C were similar, differences in their net strains and residual stresses occurred owing to thermal shrinkage after complete martensitic transformation. LTT specimen D consisted of an austenite phase with a martensite structure at room temperature, and specimen E contained an almost

fully austenitic phase. The presence of austenite was confirmed through XRD tests, and austenite peaks were detected in specimens D and E, as shown in Figure 7.

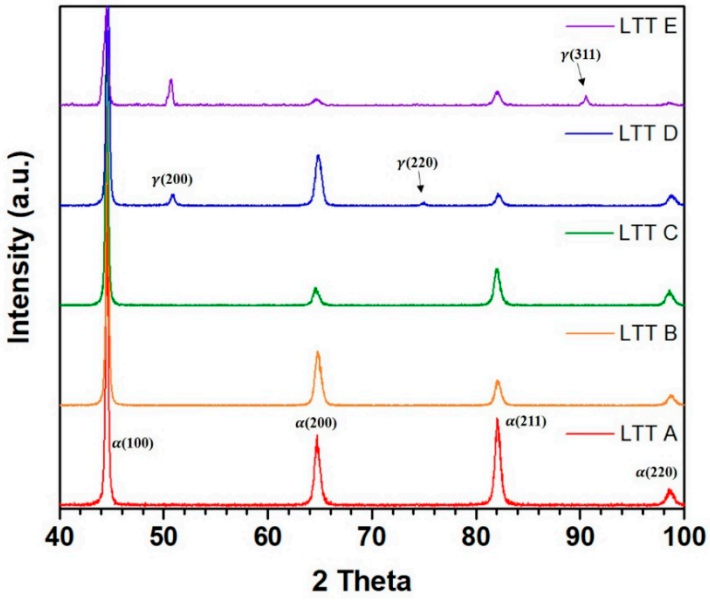


Figure 7. X-ray diffraction results of the samples.

This result could also be expected from the Schaeffler diagram, as shown in Figure 8 [25]. The matrix changes from a pure martensite matrix to a complex microstructure (austenite + martensite) as Creq and Nieq increase. The weldment is finally transformed into the austenite phase when Creq and Nieq increase sufficiently. From the dilatometer graph, the austenite phase was present in the matrix because the martensitic transformation was incomplete in the LTT specimens D and E, even at room temperature. The phase transformation of these specimens was completed with austenite remaining at room temperature because the Ms temperature was too low. Because of this, the weld could not expand to its maximum volume, the net strain and residual stress changed rapidly, and an inflection point was observed as the Ms temperature decreased.

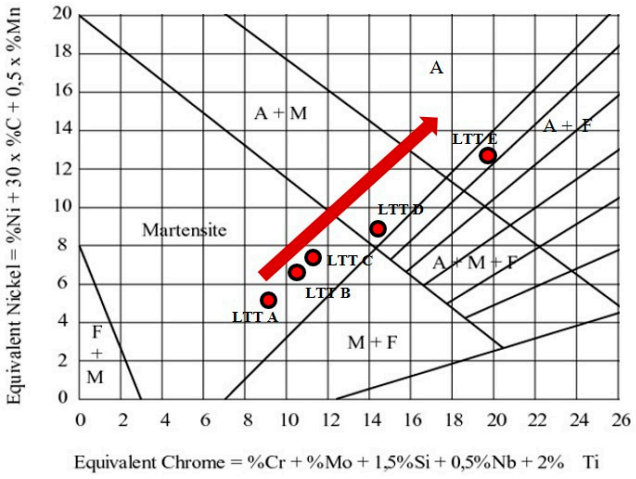


Figure 8. Phase transformation with increasing Cr and Ni content shown in a Schaeffler diagram.

In order to obtain reduced deformation of LTT weldments, the weldment should be fabricated with a matrix of martensite without any residual austenite phase. In addition, the Ms temperature should be selected corresponding to the maximum expansion point, as

a balance between shrinkage due to cooling of the transformed martensite and expansion due to the phase transformation from austenite to martensite.

4. Conclusions

In this study, the relationship between residual stress and net strain in low-temperature transformation weldments was analyzed, considering the microstructure. The results can be summarized as follows:

- Although the Creq/Nieq ratio was kept constant, the Ms temperature decreased as Creq and Nieq increased. However, at extremely low Ms temperatures the martensitic transformation of the LTT weld was not complete. Then, the expansion volume could not reach its maximum, and some austenite phase material remained in the microstructure; therefore, the characteristic low-temperature transformation was not effective.
- As the Ms temperature decreased, net strain and residual stress were presented symmetrical to each other, and both had inflection points. That is, there was a specific Ms temperature at which the maximum reduction of deformation effect could be obtained.
- Although the Ms temperature decreased with an increase in Creq and Nieq, the inflection points on the net strain and residual stress graphs were observed due to the presence of austenite at room temperature.

Author Contributions: Investigation, Y.L.; Writing—original draft, J.L.; Writing—review & editing, C.L. All authors have read and agreed to the published version of the manuscript.

Funding: This research received no external funding.

Conflicts of Interest: The authors declare no conflict of interest.

References

1. Moyer, J.M.; Ansell, G.S. The volume expansion accompanying the martensite transformation in iron-carbon alloys. *Metall. Trans. A* **1975**, *6*, 1785. [CrossRef]
2. Fahlman; Bradley, D. *Materials Chemistry*; Springer: Dordrecht, The Netherlands, 2011; pp. 1–12.
3. Wechsler, M.S.; Lieberman, D.S.; Read, T.A. On the theory of the formation of martensite. *Trans. AIME* **1953**, *197*, 1503–1515.
4. Withers, P.J.; Bhadeshia, H.K.D.H. Residual stress. Part 2—Nature and origins. *Mater. Sci. Technol.* **2001**, *17*, 366–375. [CrossRef]
5. Withers, P.J.; Bhadeshia, H.K.D.H. Residual stress. Part 1—Measurement techniques. *Mater. Sci. Technol.* **2001**, *17*, 355–365. [CrossRef]
6. Huang, T.D.; Conrardy, C.; Dong, P.; Keene, P.; Kvidahl, L.; DeCan, L. Engineering and production technology for lightweight ship structures, Part II: Distortion mitigation technique and implementation. *J. Ship Prod.* **2007**, *23*, 82–93. [CrossRef]
7. Alghamdi, T.; Liu, S. Low-transformation-temperature (LTT) welding consumables for residual stress management: Consumables development and testing qualification. *Weld. J.* **2014**, *93*, 243S–252S.
8. Kromm, A.; Kannengießer, T. Characterizing phase transformations of different LTT alloys and their effect on residual stresses and cold cracking. *Weld. World* **2011**, *55*, 48–56. [CrossRef]
9. Kromm, A.; Kannengiesser, T.; Gibmeier, J.; Genzel, C.; van der Mee, V. Determination of residual stresses in low transformation temperature (LTT-) weld metals using X-ray and high energy synchrotron radiation. *Weld. World* **2009**, *53*, 3–16. [CrossRef]
10. Kannengiesser, T.; Kromm, A. Formation of welding residual stresses in low transformation temperature (LTT) materials. *Soldag. Inspeção* **2009**, *14*, 74–81. [CrossRef]
11. Murata, H.; Katoh, N.; Tamura, H. Effect of transformation on residual stress in welding-stress releasement by transformation superplasticity (part 5). *Q. J. Jpn. Weld. Soc.* **1993**, *11*, 545–550. [CrossRef]
12. Kannengiesser, T.; Kromm, A.; Rethmeier, M.; Gibmeier, J. Residual stresses and in-situ measurement of phase transformation in low transformation temperature (LTT) welding materials. *Adv. X-ray Anal.* **2009**, *52*, 755–762. [CrossRef]
13. Gibmeier, J.; Obelode, E.; Altenkirch, J.; Kromm, A.; Kannengiesser, T. Residual stress in steel fusion welds joined using low transformation temperature (LTT) filler material. *Mater. Sci. Forum.* **2014**, 768–769. [CrossRef]
14. Ooi, S.W.; Garnham, J.E.; Ramjaun, T.I. Low transformation temperature weld filler for tensile residual stress reduction. *Mater. Des.* **2014**, *56*, 773–781. [CrossRef]
15. Wu, S.; Wang, D.; Di, X.; Zhang, Z.; Feng, Z.; Liu, X.; Li, Y.; Meng, X. Toughening mechanisms of low transformation temperature deposited metals with martensite–austenite dual phases. *J. Mater. Sci.* **2018**, *53*, 3720–3734. [CrossRef]
16. Chen, X.; Fang, Y.; Li, P.; Yu, Z.; Wu, X.; Li, D. Microstructure, residual stress and mechanical properties of a high strength steel weld using low transformation temperature welding wires. *Mater. Des.* **2015**, *65*, 1214–1221. [CrossRef]

17. Francis, J.A.; Stone, H.J.; Kundu, S.; Bhadeshia, H.K.D.H.; Rogge, R.B.; Withers, P.J.; Karisson, L. The effects of filler metal transformation temperature on residual stresses in a high strength steel weld. *J. Press. Vessel Technol.* **2009**, *131*, 041401. [CrossRef]
18. Özdemir, O.; Cam, G.; Ciemnoglu, H.; Kocak, M. Investigation into mechanical properties of high strength steel plates welded with low temperature transformation (LTT) electrodes. *Int. J. Surf. Sci. Eng.* **2012**, *6*, 157–173. [CrossRef]
19. Ohta, A.; Suzuki, N.; Maeda, Y.; Maddox, S.J. Fatigue strength improvement of lab welded joints by low transformation temperature welding wire-superior improvement with strength of steel. *Weld. World* **2003**, *47*, 38–43. [CrossRef]
20. Martinez, F. Development of a compressive residual stress field around a weld toe by means of phase transformations. *Weld. World* **2008**, *52*, 63–78.
21. An, G.; Park, J.; Han, I. Effects of high toughness and welding residual stress for unstable fracture prevention. *Appl. Sci.* **2020**, *10*, 8613. [CrossRef]
22. Ohta, A.; Suzuki, N.; Maeda, Y.; Hiraoka, K.; Nakamura, T. Superior fatigue crack growth properties in newly developed weld metal. *Int. J. Fatigue* **1999**, *21*, 113–118. [CrossRef]
23. Zenitani, S.; Hayakawa, N.; Yamamoto, J.; Hiraoka, K.; Morikage, Y.; Kubo, T.; Yasuda, K.; Amano, K. Development of new low transformation temperature welding consumable to prevent cold cracking in high strength steel welds. *Sci. Technol. Weld. Join.* **2007**, *12*, 516–522.
24. Lixing, H.; Dongpu, W.; Wenxian, W.; Yufeng, Z. Ultrasonic peening and low transformation temperature electrodes used for improving the fatigue strength of welded joints. *Weld. World* **2004**, *48*, 34–39. [CrossRef]
25. Andrews, K. Empirical formulae for some transformation temperatures. *J. Iron Steel Inst.* **1965**, *203*, 721–727.
26. Schaeffler, A.L. Constitution diagram for stainless steel weld metal. *Met. Prog.* **1949**, *56*, 680.
27. Easterling, K. *Introduction to the Physical Metallurgy of Welding*; Elsevier Ltd: Amsterdam, The Netherlands, 2013; pp. 1–54.
28. Zhou, W.; Zhou, H.; Zhang, R.; Pei, Y.; Fang, D. Measuring residual stress and its influence on properties of porous ZrO_2/(ZrO_2+Ni) ceramics. *Mater. Sci. Eng. A* **2015**, *622*, 82–90. [CrossRef]
29. Mathar, J. Determination of initial stresses by measuring the deformation around drilled holes. *Trans. ASME* **1934**, *56*, 249–254.
30. Mochizuki, M.; Hayashi, M.; Hattori, T. Numerical analysis of welding residual stress and its verification using neutron diffraction measurement. *J. Eng. Mater. Technol.* **2000**, *122*, 98–103. [CrossRef]
31. Bahadur, A.; Kumar, B.R.; Kumar, A.S.; Sarkar, G.G.; Rao, J.S. Development and comparison of residual stress measurement on welds by various methods. *Mater. Sci. Technol.* **2004**, *20*, 261–269. [CrossRef]
32. Beaney, E.M. Accurate measurement of residual stress on any steel using the center hole method. *Strain* **1976**, *12*, 99–106. [CrossRef]
33. Kujanp, V.; Suutala, N. Correlation between solidification cracking and microstructure in austenitic and austenitic-ferritic stainless steel welds. *Weld. Res. Int.* **1979**, *9*, 55–75.
34. ASTM A1033-18. *Standard Practice for Quantitative Measurement and Reporting of Hypoeutectoid Carbon and Low-Alloy Steel Phase Transformations*; ASTM International: West Conshohocken, PA, USA, 2018; Available online: https://www.astm.org (accessed on 12 April 2021).
35. Kamyabi-Gol, A.; Herath, D.; Mendez, P.F. A comparison of common and new methods to determine martensite start temperature using a dilatometer. *Can. Metall. Q.* **2017**, *56*, 85–93. [CrossRef]
36. Lee, J.; Kim, D.; Lee, Y.; Lee, C. Influence of alloying elements in low transformation temperature weldment on Ms. temperature, microstructure and mechanical properties. *Mater. Charact.* **2021**, *171*, 110755. [CrossRef]